Effect of molecular weight of tyramine-modified hyaluronan on polarization state of THP-1 and peripheral blood mononuclear cells-derived macrophages

Jacek K. Wychowaniec,*[a] Ezgi Irem Bektas,[a] Andrea J. Vernengo,[a,δ] Marcia Mürner,[a,b] Marielle Airoldi,[a] Paul Sean Tipay,[c] Jiranuwat Sapudom,[d] Jeremy Teo,[d] David Eglin[e] and Matteo D'Este[a]

[a] AO Research Institute, Clavadelerstrasse 8, Davos, 7270, Switzerland

[b] ETH Zürich, Zürich, 8093, Switzerland

[c] Independent Scholar

[d] Laboratory for Immuno Bioengineering Research and Applications, Division of Engineering, New York University Abu Dhabi, Abu Dhabi, 129188, United Arab Emirates

[e] Mines Saint-Étienne, Univ Jean Monnet, INSERM, U1059 Sainbiose, Saint-Étienne, France

[δ] Current address: Henry M. Rowan College of Engineering, Department of Chemical Engineering and Biomedical Engineering, Rowan University, Glassboro, NJ, USA

*Corresponding author J.K.W.
Phone: (+41)0779238956; e-mail: jacek.wychowaniec@aofoundation.org

Graphical Abstract

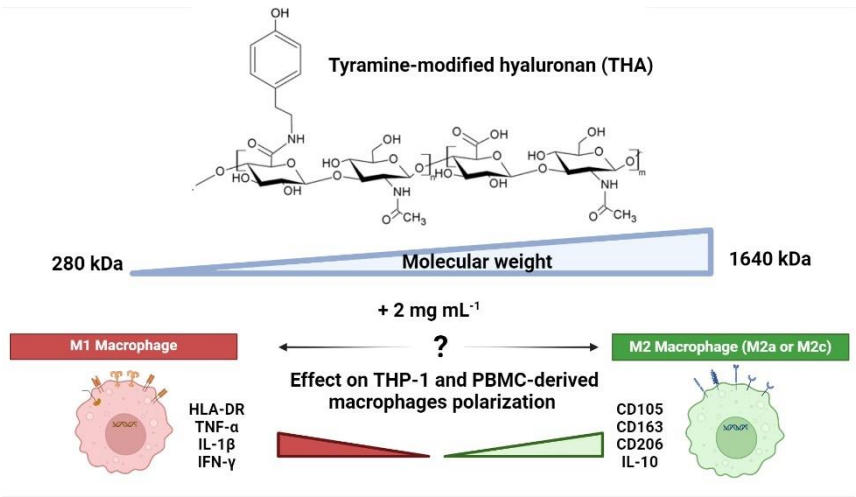

Abstract

The immunomodulatory properties of hyaluronan and its derivatives are key to their use in medicine and tissue engineering. In this work we evaluated the capability of soluble tyramine-modified hyaluronan (THA) of two molecular weights (low M_w=280 kDa and high M_w=1640 kDa) for polarization of THP-1 and peripheral blood mononuclear cells (PBMCs)-derived macrophages (MΦs). We demonstrate the polarization effects of the supplemented THA by flow cytometry and multiplex ELISA for the THP-1 derived MΦs and by semi-automated image analysis from confocal microscopy, immunofluorescent staining utilising CD68 and CD206 surface markers, RT-qPCR gene expression analysis, as well as using the enzyme-linked immunosorbent assay (ELISA) for PBMCs-derived MΦs. Our data indicates that supplementation with LMW THA drives changes in THP-1 derived MΦs towards a pro-inflammatory M1-like phenotype, whereas supplementation with the HMW THA leads to a more mixed profile with some features of both M1 and M2 phenotypes, suggesting either a heterogeneous population or a transitional state. These states could not be clearly identified for PMBCs-derived MΦs, pointing out a differential regulation of factors including IL-10 and CD206 between the two cell sources. While human primary cells add to the clinical relevance,

donor diversity introduces wider variability in the dataset, preventing drawing strong conclusions. Nevertheless, the MΦs profiles observed in THP-1 derived cells for treatments with LMW and HMW THA are generally consistent with what might be expected for the treatment with non-modified hyaluronans of respective molecular weights, confirming the known association holds true for the chemically tyramine-modified hyaluronan. We stipulate that these responses will provide basis for more accurate *in vivo* representation and translational immunomodulatory guidance for the use of THA-based biomaterials to a wider biomaterials and tissue engineering communities.

Keywords: Tyramine-modified hyaluronan; THP-1-derived macrophages; Peripheral blood mononuclear cells-derived macrophages; Macrophage Polarization; Inflammation; Immunomodulation

1. Introduction

The ability to generate and control a variety of individualized cellular signals plays a vital role in the design of biopolymers for biomedical applications. It is well established that the immune system is vital in inducing normal healing of damaged tissues, mediated by both innate and adaptive immunity, mainly by inflammation [1-5]. During injury, the immune system can have both beneficial and detrimental effects that improve tissue repair or escalate degeneration, in a context-dependent manner [6-9]. These opposing effects are associated with the phenotypic state of the immune cells present at the injury site. The complexity of cell types and signalling pathways involved in inflammatory and/or degenerative processes encompasses a vast array of immune cells, including T cells, B cells, dendritic cells, monocytes, neutrophils and macrophages (MΦs), as well as cytokines, chemokines, growth factors, and molecular interactions between all components, creating a highly intricate and multifaceted network that orchestrates the progression and resolution of any pathological process [10, 11]. MΦs are often considered among the most important immune cells due to their versatile and central role in the immune system, particularly by their key role in producing a wide range of cytokines and chemokines that drive subsequent clearance and tissue resolution [12]. In the last decade new MΦ subtypes were discovered as part of innate immunity and have been shown to play crucial regulatory role in successful tissue regeneration [13]. MΦs thus exist in a spectrum of polarization that ranges from a pro-inflammatory and detrimental M1 state to protective anti-inflammatory M2 states [7, 9, 14-16]. M1 MΦs are activated in response to pathogens, such as interferon-gamma (IFN-γ) and lipopolysaccharides (LPS) from bacteria, produce high levels of pro-inflammatory cytokines (IL-1β, IL-6, and TNF-α) and nitric oxide, efficiently present antigens to T helper 1 (Th1) cells, and overall promote inflammation and host defence. On the other hand, M2 MΦs are activated in response to anti-inflammatory signals (including IL-4, IL-13, IL-10, and glucocorticoids), are involved in tissue remodelling, producing arginase-1,

and promoting wound healing and immunosuppression [13, 17]. Overall surface markers including CD163, CD206, and CD209 are characteristic of M2 activations [13, 18]. In general, the relative abundance of these MΦ phenotypes can shift dynamically during the course of tissue damage and repair, with M1 state mostly present in early inflammatory phase of an acute injury and M2 appearing through resolution and repair phase. Hence, time-dependent immunomodulation towards a certain state offers the opportunity to enhance functional recovery [19, 20]. Typical immune signalling pathways convert external stimuli into cytosolic events that lead to the resolution of infection, associated with downstream adaptors and effectors undergoing substantial conformational changes and spatial reorganization upon ligand engagement [21, 22]. Importantly, this process can be also achieved by: i) the use of appropriate materials providing biochemical and physical cues, or ii) by therapeutic administration of immunomodulatory molecules [23]. The final MΦ fate is driven by the complex interplay between external environmental signals and hardwired differentiation programming capabilities. In light of this, many recent studies have shown that certain biomaterials have inherent immunomodulatory properties capable of reducing the damaging innate inflammatory response caused by MΦ infiltration, both *in vitro* and *in vivo* [24-26]. For example, engineered matrices enriched in immunomodulatory factors were shown to induce enhanced bone formation by promoting higher vascular invasion and instructed earlier inflammation [25].

Hyaluronan (HA) is a linear, anionic polysaccharide known to play a major biological role in a range of human tissues [27], and it has been employed in a plethora of applications as biomaterial and in tissue engineering [28-31]. Depending on its modal molecular weight (M_w) and extrinsic environment, HA has been shown to influence multiple biological pathways, including influencing paracrine signalling of neighbouring immune cells [32-34]. This occurs through HA interactions with RHAMM (receptor for HA mediated motility) and CD44

principal receptors [35]. Particularly, CD44 receptor can distinguish the M_w of HA and subsequently deliver contradictory signals to active different biological processes through clustering effects [36]. For example Rayahin *et al.* demonstrated on murine MΦs (J774A.1) that high molecular weight (>1000 kDa) HA can polarize them to an M2-like phenotypes, whereas low molecular weight HA (<1000 kDa) drives pro-inflammatory M1-like polarization [37]. More recently Lee *et al.* have concurred with original work demonstrating that high molecular-weight HA (>1250 kDa) inhibited pro-inflammatory responses in lipopolysaccharides (LPS)-stimulated RAW 264.7 murine MΦs and in concentration-dependent way induced anti-inflammatory responses [38]. Whilst many effects hold true for the mice or rat-derived MΦs, typically polarization state are more variable in human-derived cells due to known donor variability [39-41]. The effects of HA M_w on its biological properties have been widely investigated, sometimes with contradictory reports, and this variability has been attributed to different HA sources and impurities, mainly endotoxin, introducing bias [39, 40, 42]. In one case, the high molecular weight HA (M_w=1010–1800 kDa) triggered an effective polarization of primary human monocytes (THP-1 cells) towards an M2-like state [43]. To date variable results were noted, with an overall polarization of MΦs to HA depending on the exact cell type and source, concentration, M_w and associated endotoxin levels. These however have not been provided for chemically functionalized versions of HA, which are more commonly used across tissue engineering and regenerative medicine fields.

Recently, tyramine-modified hyaluronan (THA) has gained prominence as biopolymer and building block of therapeutic biomaterials enabling rapid biofabrication and cellular attachment by means of both enzymatic (horseradish peroxidase, H_2O_2) and light-based crosslinking (e.g. Eosin and green light irradiation) methods [44-48]. THA has also been used in conjugation with collagen as an extrudable bioink with internal architecture and inducing cellular alignment and migration [49]. Recently part of our group investigated the effect of

THA (M_w=280 kDa) hydrogels along various other biomaterials, on neutrophils, indicating relative immuno-inertness and lack of enhanced pro-inflammatory response compared to other studied materials [24].

We stipulate that designing functional biomaterials that incorporate immunomodulatory effects, biocompatibility and that allow stable long-term polarization of MΦs is therefore of high interest in tissue engineering and biofabrication fields [23], and hence in the current work we evaluated the capability of MΦ polarization of THA of two molecular weights: M_w=280 kDa (LMW THA) and M_w=1640 kDa (HMW THA), supplemented in cell culture medium at a 2 mg mL^{-1} concentration, in the typical range observed in human knee synovial fluid [50], as a soluble signal. Such signal is expected to: (i) occur as a released factor from three-dimensional THA-based crosslinked biomaterials, with 2 mg mL^{-1} an estimated concentration from leaching hydrogels fragments, e.g. 10% degradation rate of a hydrogel containing 20 mg mL^{-1} in a short amount of time [51], or (ii) be used as simple carbohydrate supplementation to medium. The polarization effects of the supplemented THA on MΦs differentiated from two distinct sources, genetically similar THP-1 cells, as well as human peripheral blood mononuclear cells (PMBCs) from three donors, were evaluated. M1-like and M2-like polarization modulated by the supplementation with THA were assessed by the flow cytometry and multiplex ELISA for the THP-1-derived MΦs and by immunofluorescent staining, gene expression analysis and ELISA for PBMCs-derived MΦs.

2. Materials and methods

2.1. Synthesis and characterisation of tyramine-modified hyaluronan (THA)

THA of two molecular weights: M_w=280 kDa (abbreviated throughout as LMW THA) and M_w=1640 kDa (abbreviated throughout as HMW THA) were synthesized as previously described [46, 52]. Briefly, sodium hyaluronate (Contipro Biotechs.r.o., Czech Republic) was dissolved in deionized H_2O at 1 w/v%. THA conjugates were prepared in a one-step reaction

by addition of 1.25 mmol 4-(4,6-dimethoxy-1,3,5-triazin-2-yl)-4-methylmorpholinium chloride (DMTMM, TCI Europe N.V.) coupling agent and subsequently 1.25 mmol tyramine hydrochloride (Roth, 5234.3) was added dropwise to the solution. The reaction was carried out at 37 °C and under continuous stirring for 24 h. The product was purified via precipitation with 96% ethanol after the addition of 10 v/v% saturated sodium chloride. Several wash steps were performed, and the product kept under vacuum for 72 h, with first 24 h at 25°C and then for two final days at 40°C. For HMW THA, the purification and washing were repeated twice to ensure complete removal of trapped H_2O and ethanol. Proton nuclear magnetic resonance spectroscopy (^{1}H NMR, 300 MHz, Bruker Avance III) and UV absorbance measurements at 275 nm on Infinite® 200 Pro plate reader (Tecan, Männedorf, Switzerland) were performed to confirm the degree of substitution (DoS) of tyramine on HA (with $DoS_{LMW\ THA}$= 6.01 ± 0.57 %, and $DoS_{HMW\ THA}$= 5.99 ± 0.57 %). ^{1}H NMR data is presented in ***Figure S1***. Loss of drying (LOD) was also evaluated. For that, 100 mg of THA was weighted into a glass vial and dried under vacuum at 105°C for 24 h. LOD was then calculated following the formula:

$$\text{LOD (\%)} = \frac{W_b - W_a}{W_b} \times 100\% \qquad (1)$$

, where W_b defines weight of THA before drying and W_a defines weight of THA after drying. The following values were obtained: $LOD_{LMW\ THA}$= 9.8 ± 0.5 %, and $LOD_{HMW\ THA}$= 12.8 ± 0.5 %.

2.2. Endotoxin analysis

Bacterial endotoxins (lipopolysaccharides, LPS)-cell wall material from gram negative bacteria is a commonly known molecule that can activate immune cells [53]. To evaluate the LPS content of THA, the endotoxin content was measured using the Pierce™ Chromogenic Endotoxin Quant Kit (Thermo-Fisher) according to the manufacturer's instructions. To evaluate THA, we adapted our previous protocol [24], and prepared enzymatically crosslinked THA hydrogels at 3.5 w/v% with 0.1 U mL^{-1} Horseradish peroxidase (HRP) 0.15 mM H_2O_2,

the same for both LMW and HMW THA. The THA hydrogels were directly prepared in the wells and were incubated for 1 hour with endotoxin free H_2O (Sigma-Aldrich). An endotoxin standard stock solution was prepared by adding endotoxin free H_2O (Sigma-Aldrich) to the E. coli endotoxin standard vial to create a high standard (0.1-1.0 EU mL^{-1}) and a low standard (0.01-0.1 EU mL^{-1}). After 1 hour the supernatant H_2O was harvested from the THA hydrogels and transferred to the pre-warmed readout plate at 37 °C as well as two standard curves were prepared on this plate. The amoebocyte lysate reagent was added to each well and the plates were incubated for 8 min at 37 °C. The reaction of the chromogenic substrate solution was stopped after 6 min at 37 °C by adding 25 v/v% acetic acid to each well and the optical density was measured at 405 nm using the Infinite® 200 Pro plate reader (Tecan, Männedorf, Switzerland). The obtained values were used to calculate the concentration based on the provided standard curve for the aforementioned concentration ranges, with R^2=0.98 and R^2=0.95 for low and high standards, respectively.

2.3. Quantification of the pro-inflammatory response of monocytes via NFKB expression

THP-1 monocytic cells with the NFκB-GFP reporter gene were kindly provided by Dr. Xin Xie (Core Technology Platform, New York University Abu Dhabi, UAE). The cells were cultured in RPMI-1640 media supplemented with 10% fetal bovine serum (FBS), 1% sodium pyruvate, 0.01% mercaptoethanol, and 1% penicillin/streptomycin at 37°C, 5% CO_2, and 95% humidity. Cell culture media and supplements were purchased from Gibco™ (Thermo Fisher Scientific, Inc., Dreieich, Germany). To quantify the pro-inflammatory response, 5×10^5 cells were cultured with or without at 2 mg mL^{-1} THA (10 times diluted from originally prepared THA hydrogels at 20 mg mL^{-1} with 0.1 U mL^{-1} Horseradish peroxidase (HRP) 0.15 mM H_2O_2), for 24 hours under standard cell culture conditions. As a positive control, the cells were treated with 10 ng mL^{-1} TNF-α (Biolegend, San Diego, CA, USA), known to activate NFκB signalling pathway. Cells were also treated with 10 ng mL^{-1} IFN-γ, as it is a known to confirm specificity

of control because it does not trigger NFkB signalling pathway. Subsequently, the cells were analysed using an Attune NxT Flow Cytometer equipped with an autosampler (Thermo Fisher Scientific, Inc., Dreieich, Germany). Data analysis was performed using FlowJo software (Becton, Dickinson and Company, Franklin Lakes, NJ, USA). The geometric mean fluorescence intensity (gMFI) of the NFκB-GFP reporter was evaluated. Experiments were performed in 5 replicates.

2.4. MΦ differentiation from THP-1 cells and treatment with the soluble THA

For MΦ differentiation, 1×10^5 THP-1 cells (ATCC, Manassas, VA, USA) were incubated with 300 nM phorbol 12-myristate 13-acetate (PMA; Sigma-Aldrich, Darmstadt, Germany) in RPMI-1640 media supplemented with 1% sodium pyruvate, 0.01% mercaptoethanol, and 1% penicillin/streptomycin but without fetal bovine serum (FBS), following previously published protocols [54, 55]. The cell culture media and supplements were acquired from Gibco™ (Thermo Fisher Scientific, Inc., Dreieich, Germany). After 6 h, the differentiation medium was removed, and the cells were allowed to rest for 24 h in RPMI-1640 without FBS and PMA. Subsequently, the differentiated MΦs were cultured either with or without 2 mg mL^{-1} THA (10 times diluted from originally prepared THA hydrogels at 20 mg mL^{-1} with 0.1 U mL^{-1} HRP 0.15 mM H_2O_2), for 48 h. As a control, MΦs were activated into pro-inflammatory (M1) MΦs for 48 h by adding 10 pg mL^{-1} lipopolysaccharide (LPS; Sigma, USA) and 20 ng mL^{-1} interferon-gamma (IFN-γ; Biolegend, San Diego, CA, USA). For anti-inflammatory activation, MΦs were induced into the M2a subtype with 20 ng mL^{-1} interleukin 4 (IL-4; Biolegend, USA) and 20 ng mL^{-1} interleukin 13 (IL-13; Biolegend, USA), or into the M2c subtype with 20 ng mL^{-1} interleukin 10 (IL-10; Biolegend, USA).

2.5. Quantitative analysis of THP-1-derived MΦs cell surface markers and their cytokine secretion profile

For analysis of MΦ cell surface markers, MΦs were detached from the cell culture plates using Macrophage Detachment Solution DXF (PromoCell, Heidelberg, Germany) following incubation with 2 mg mL^{-1} THA (10 times diluted from originally prepared THA hydrogels at 20 mg mL^{-1} with 0.1 U mL^{-1} HRP 0.15 mM H_2O_2). Before cell staining, they were incubated with Human TruStain FcX™ – Fc Receptor Blocking Solution (5 μL of blocking solution in 1000 μL of staining volume; Biolegend, San Diego, CA, USA) for 5 min under standard cell culture conditions. Subsequently, the cells were stained with mouse anti-human HLA-DR (clone: L243) conjugated with Brilliant Violet 421, CD163 (Clone: GHI/61) conjugated with PE-Cy7, mouse anti-human CD206 (Clone: 15-2) conjugated with Brilliant Violet 510, and DRAQ7 (a cell viability staining dye) for 30 min on ice. The antibodies and DRAQ7 dye were diluted in PBS at a 1:250 ratio. All antibodies used in this study were sourced from Biolegend, San Diego, CA, USA. The stained cells were then analysed using an Attune NxT Flow Cytometer equipped with an autosampler (Thermo Fisher Scientific, Inc., Dreieich, Germany), with compensation settings adjusted prior to analysis. Data analysis was conducted using FlowJo software (Becton, Dickinson and Company, Franklin Lakes, NJ, USA), focusing on the geometric mean fluorescence intensity of the cell surface markers. Experiments were performed in 5 replicates. For cytokine secretion profile analysis, cell culture supernatants were harvested following incubation with THA as already described. The cytokine levels were quantified using a bead-based multiplex immunoassay (LEGENDplex™ Human Essential Immune Response Panel; Biolegend, San Diego, CA, USA) designed for IL-4, IL-2, CXCL10 (IP-10), IL-1β, TNF-α, CCL2 (MCP-1), IL-17A, IL-6, IL-10, IFN-γ, IL-12p70, CXCL8 (IL-8), and TGF-β1, according to the manufacturer's protocol. The samples were analysed on an Attune NxT Flow Cytometer (Thermo Fisher Scientific, Carlsbad, CA, USA). Data were processed using a 5-parameter curve fitting algorithm with LEGENDplex™ data analysis software (Biolegend, San Diego, CA, USA), and experiments were performed in 5 replicates.

2.6. MΦ differentiation from peripheral blood mononuclear cells (PBMCs) and treatment with the soluble THA

Primary human monocytes were isolated from buffy coats purchased from the Regional Blood Donation Service SRK Graubünden (Chur, Switzerland) from three human donors (D1, D2 and D3) using Ficoll density gradient separation. No donor information was received as per local regulations. Obtained peripheral blood mononuclear cells (PMBCs) were labelled with CD14 magnetic beads followed by magnetic-activated cell sorting (MACS) [56, 57]. $CD14^+$ monocytes cells were resuspended in RPMI medium supplemented with 10% FBS and then seeded onto tissue culture plastic at a density of 1.82 x 10^5 cells $well^{-1}$ for D1, and at a density of 3.0 x 10^5 cells $well^{-1}$ for donors D2 and D3, both in the presence of 20 ng mL^{-1} human macrophage colony-stimulating factor (hM-CSF) for 5 days. Medium (still containing hM-CSF) was exchanged on day 2. At day 5, hM-CSF-free medium was supplemented with 10 ng mL^{-1} TNF-α and IFN-γ for M1 MΦs and 10 ng mL^{-1} IL-4 for M2MΦs for 24 h followed by a 24-hour rest in medium without cytokines (***Figure 3A***). M0-like MΦs control samples were cultured in medium without any cytokines (***Figure 3A***). Furthermore, on day 5, the same three polarization states were maintained (M0, M1, M2), either without any external influence of materials, or in the presence of the 2 mg mL^{-1} LMW THA and HMW THA supplemented in the cell culture medium (***Figure 3A***). Noteworthy, 2 mg mL^{-1} of both LMW and HMW THA remained liquid and did not result in a formation of any self-supporting physical hydrogels. On day 7, conditioned medium was collected, samples were washed two times with PBS and fixed with 4% formaldehyde for 20 min for immunofluorescent staining and stored in TRI-reagent for subsequent RNA isolation (***Figure 3A***).

2.7. Immunofluorescence analysis

D1 samples for immunofluorescent analysis were stained for nucleus with DAPI (NucBlue® Fixed Cell ReadyProbes® Reagent, ThermoFisher), and for phalloidin (ActinGreen™ 488

ReadyProbes® Reagent, ThermoFisher). Samples were firstly permeabilized with 0.25% Triton X-100 in PBS for 30 min and subsequently washed two times with wash buffer (0.05% Tween-20 in PBS). Samples were then firstly stained with phalloidin and left for 1 h in darkness. Subsequently, they were washed again two times with wash buffer, and finally incubated with DAPI for 10 min in darkness. Manufacturers' instructions were followed for DAPI and ActinGreen dilutions (1 drop per 0.5 mL).

D3 samples for immunofluorescent analysis were stained for nucleus with DAPI (NucBlue® Fixed Cell ReadyProbes® Reagent, ThermoFisher), for phalloidin (ActinRed™ 555 ReadyProbes® Reagent, ThermoFisher), for MMR/CD206 (M2a MΦ surface marker) with Alexa Fluor® 700 (FAB25342N, R&DSystems, Bio-Techne), and for CD68/SR-D1 (a glycoprotein marker that is primarily found on the surface of MΦs) with Alexa Fluor® 488 (IC20401G, R&DSystems, Bio-Techne). Samples were firstly permeabilized with 0.25% Triton X-100 in PBS for 30 min and subsequently washed once with wash buffer. Samples were then firstly stained with phalloidin and left for 3 h in darkness. Subsequently, they were washed one time with wash buffer, and then incubated with blocking solution (1% BSA in 1x PBS) for 1 h. Then samples were washed one time with wash buffer and incubated with CD68 or CD206 staining (separate wells) pre-made at 8 µg mL^{-1} with 0.1% BSA in PBS overnight in darkness. Subsequently samples were washed one more time with wash buffer and incubated with DAPI for 10 min. Manufacturers' instructions were followed for DAPI and ActinRed dilutions (1 drop per 0.5 mL). D2 samples were used to establish the appropriate staining protocol, subsequently used, and described above for D3 samples.

Samples were analysed using confocal microscope (Zeiss LSM800 Airyscan Confocal Microscope) with channels at 405 nm (DAPI), 561 nm (ActinRed), 515 nm (ActinGreen/CD68 Alexa Fluor 488) and 723 nm (CD206, Alexa Fluor 700).

Image analysis (nucleus cell area and circularity, cells area as well as CD68 area) was performed using ImageJ® on images taken using 10x objective. Only areas in the range from 5 to 120 μm^2 and 90 to 400 μm^2 were taken into consideration, for nucleus and cell, respectively. For CD68 analysis, 10 to 400 μm^2 areas were taken into consideration. Smaller areas would be indicative of fragments whereas larger were excluded based on threshold found in manual analysis indicating more than 2 nuclei/cell of cells overlapping with each other/touching.

2.8. RNA isolation and RT-qPCR gene analysis of PBMCs-derived MΦs

To assess the polarization of MΦs, cells were collected and seeded in a 24-well plate at a concentration and with treatments described in section 2.6. RNA was isolated with salt precipitation. The obtained RNA content ranged from 420 to 1240 ng (***Table S1***). TaqManTM Reverse Transcription Kit was used to generate cDNA. Relative gene expression reactions were set up in 10 µL reaction mixes using TaqManTM MasterMix relevant human primers (***Table 1***), diethyl pyrocarbonate treated water (DEPC-water) and cDNA (10 ng). Real-time polymerase chain reaction (real-time PCR) was performed on two technical duplicates for n=4 (D1) or n=3 (D2 and D3) repeats, using QuantStudio 7 Flex. The relative gene expression was identified $\log_2$(fold change), where fold change = $2^{-\Delta\Delta Ct}$ value with RPLP0 as endogenous control and M0 MΦs with no supplemented material as control were used for normalization.

Table 1. Human primer sequences for real-time PCR

MARKER	ASSAY ID (THERMOFISHER)	ROLE
TNF-α	Hs00174128_m1	Pro-inflammatory marker (associated with M1 MΦs)
IL-6	Hs00174131_m1	
IL-1β	Hs00174097_m1	
INOS	Hs01075529_m1	
IL-10	Hs00961622_m1	Anti-inflammatory marker (associated with M2b-d MΦs)
CD206	Hs00267207_m1	M2a/M2c MΦ surface marker
CD163	Hs00174705_m1	M2c MΦ surface marker
RPLP0	Forward: *5'-TGG GCA AGA ACA CCA TGA TG-3'*	Housekeeping gene

Reverse: *5'-CGG ATA TGA GGC AGC AGT TTC-3'* Probe: *5'-AGG GCA CCT GGA AAA CAA CCC AGC-3'*

2.9. Enzyme-linked immunosorbent assay (ELISA) of PBMCs-derived MΦs

At the end of each polarization experiment, supernatant media was collected and kept for measurements of pro-inflammatory (IL-1β, IL-6, TNF-α), anti-inflammatory (IL-10) cytokines and anti-inflammatory surface receptor marker associated with M2c MΦs (CD163). The DuoSet ELISA systems were used according to the manufacturer's instructions (DY201, DY206, DY210, DY1607, DY217B, R&D Systems, respectively). Absorbance values were measured on Infinite® 200 Pro plate reader (Tecan, Männedorf, Switzerland) at 450 nm with a background wavelength correction of 540 nm.

2.10. Statistical analysis

All results were analysed and presented with GraphPad Prism version 9.3.1. Results are shown as an average ± standard deviation (SD), with individual points marked. To perform statistical significance one-way analysis of variance (ANOVA) with Šídák's multiple comparisons, Tukey's multiple comparisons test, or Kruskal-Wallis multiple comparisons or two-way analysis of variance (Anova) with mixed effects were used and noted in each case in Figure description. A statistically significant results were considered as of $p<0.05$ (ns - >0.05, * - <0.05, ** - <0.01, *** - <0.005 and **** - <0.001).

3. Results and discussion

3.1. Endotoxins analysis

To eliminate the possible effects stemming from the endotoxins, we confirmed that their measured levels were 0.27 ± 0.07 U mL^{-1} and 0.26 ± 0.04 U mL^{-1} for LMW THA and HMW THA, respectively, below the limit for clinical medical devices of 0.5 EU mL^{-1} set by the USA Food and Drug Administration (FDA) [58]. Given that endotoxin levels were similar for both LMW and HMW THA, we anticipate that any unravelled differences due to THA in polarisation experiments discussed throughout this article will stem solely from the difference in M_w.

3.2. Immunological effects exerted on genetically similar monocytic THP-1 cells-derived MΦs

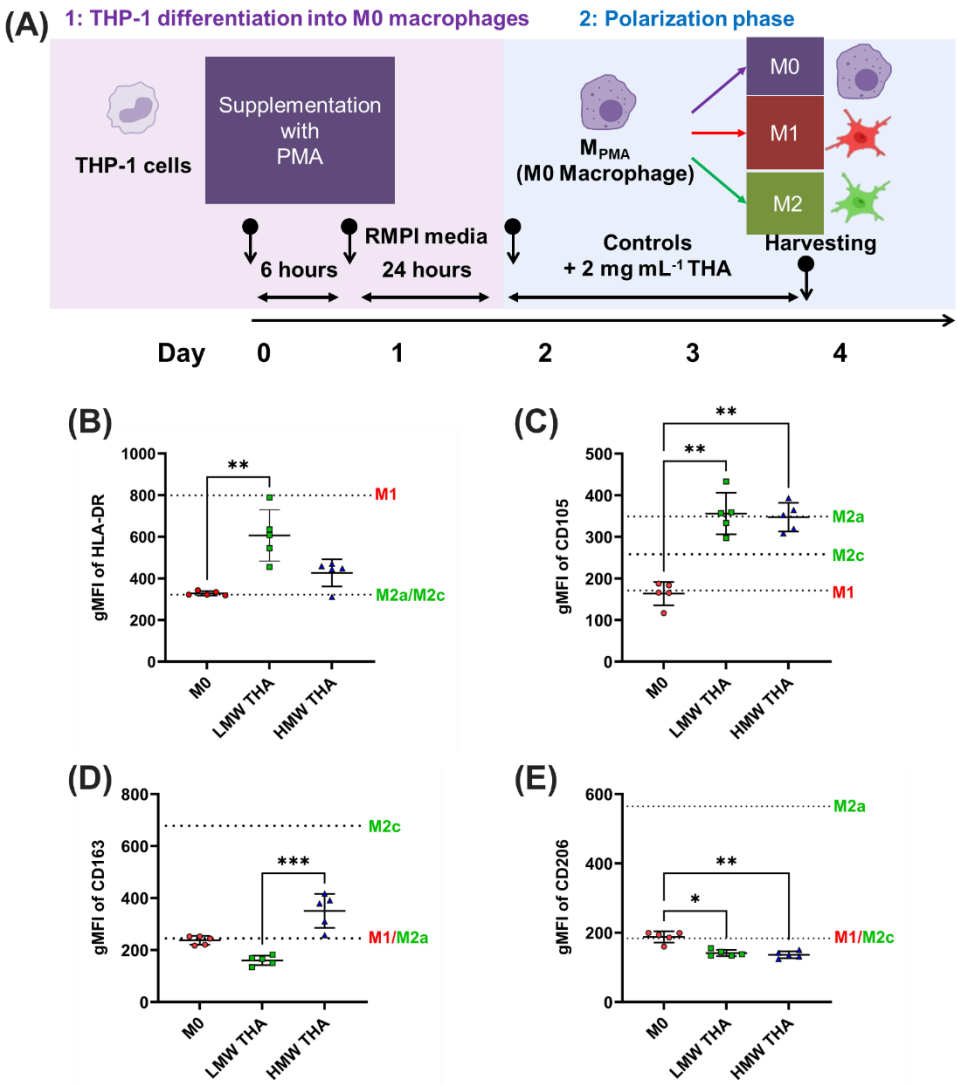

Figure 1. (A) *Scheme summarizing the differentiation protocol of THP-1-derived MΦs. THP-1 cells were differentiated into M0 MΦs by treatment with 300 nM phorbol-12-myristate-13-acetate (PMA) for 6 hours, followed by resting for 24 h in cell culture media. Subsequently, M0 MΦs were cultured in the presence of the 2 mg mL^{-1} supplemented in the cell culture medium for 48 h. Quantitative analysis of cell surface markers of* ***(B)*** *HLA-DR,* ***(C)*** *CD105,* ***(D)*** *CD163 and* ***(E)*** *CD206. Geometric mean fluorescence intensity (gMFI) was plotted. Black line and error bar in the plot represent mean and standard deviation, respectively. In all cases* ***(B-E)****, horizontal dashed lines depict average values for the control polarized MΦs obtained as indicated in methods section. Statistical analysis in* ***(B-E)*** *was done by Kruskal-Wallis multiple comparisons test. A statistically significant results were considered for p<0.05 (* - <0.05, ** - <0.01, *** - <0.005 and **** - <0.001).*

Firstly, we evaluated the effects of supplemented THA on genetically similar THP-1 monocytic cells that carried the NFκB-GFP reporter gene and we tested whether supplementation has any capacity to activate NFκB signalling pathway (***Figure S2***), which is well correlated with the induction of pro-inflammatory responses [26, 59]. Genetically similar

THP-1 cells enable screening of immunomodulation potential by minimizing any biological variability stemming from primary human cells. Cells treated with IFN-γ, which is known not to trigger this pathway, as well as cells supplemented with LMW and HMW THA did not show any significant upregulation as compared to untreated cells, and hence do not trigger any obvious pro-inflammatory response in this model under the tested conditions. Out of all tested samples, only when cells were treated with TNF-α, this pathway was activated as evidenced by significantly higher geometric mean fluorescent signal intensities ($p<0.005$) as compared to untreated cells (***Figure S2***) [60].

3.2.1. Flow cytometry profiling of THP-1 derived MΦ phenotypes

Next, following the protocol established by Sapudom *et al.* [54], we investigated the general polarization capacity of THA on THP-1-derived MΦs (***Figure 1A***). MΦ phenotypes were characterized by flow cytometry using four specific surface markers: HLA-DR for pro-inflammatory MΦs (M1), CD105 for anti-inflammatory MΦs (M2), and subsequently CD163 for anti-inflammatory MΦs (M2c) and CD206 for anti-inflammatory MΦs (primarily for M2a/M2c) sub-phenotypes [61, 62]. Control M1 and M2 subtypes (M2a and M2c) are also presented in all graphs as horizontal lines. We observed significantly higher abundance of HLA-DR surface markers ($p<0.01$) for cells encapsulated with LMW THA (***Figure 2B***). Pro-inflammatory MΦs typically exhibit HLA-DR expression levels approximately 5- to 10-fold higher than those seen in anti-inflammatory MΦs, whether derived from PBMCs or THP-1 cells [62, 63]. Hence, it appears that LMW THA stimulates a pro-inflammatory polarization capacity in our model. On the other hand, we did not see any significant difference for HMW THA as compared to M0 control (***Figure 2B***). We then noticed significantly higher abundance of $CD105^{+}$ cells ($p<0.01$) when encapsulated both with LMW and HMW THA (***Figure 1C***), generally indicating cell involvement in angiogenesis and tissue repair processes [55, 61].

Given the importance of the M2 subtypes in tissue resolution, next we evaluated specific surface receptors, including CD163 (***Figure 1D***) and CD206 (***Figure 1E***), known to be associated primarily with M2c and M2a subtypes, respectively. Significant upregulation of $CD163^{+}$ receptor ($p<0.005$) was found for cells supplemented with HMW THA, as compared to LMW THA (***Figure 1D***). At the same time, significantly lower abundance of $CD206^{+}$ cells were observed for both LMW THA ($p<0.05$) and HMW ($p<0.01$), as compared to untreated cells (***Figure 1E***).

In summary, flow cytometry suggests that both LMW and HMW THA treatments lead to upregulation of CD105, suggesting a common involvement in tissue repair and angiogenesis, possibly stemming from the common chemistry of both molecules. However, they differ in their effects on HLA-DR, CD163, and CD206 expression, indicating differences in pro-inflammatory activation (M1) and M2c MΦ polarization, both deviating from standard M2a MΦ subtype. This points towards the fact that HMW THA may stimulate differentially the MΦs towards a number of states, including the tissue reparative state and promotion of the healthy restoration of normal tissue architecture [55].

3.2.2. Multiplex ELISA profiling of THP-1 derived MΦ phenotypes

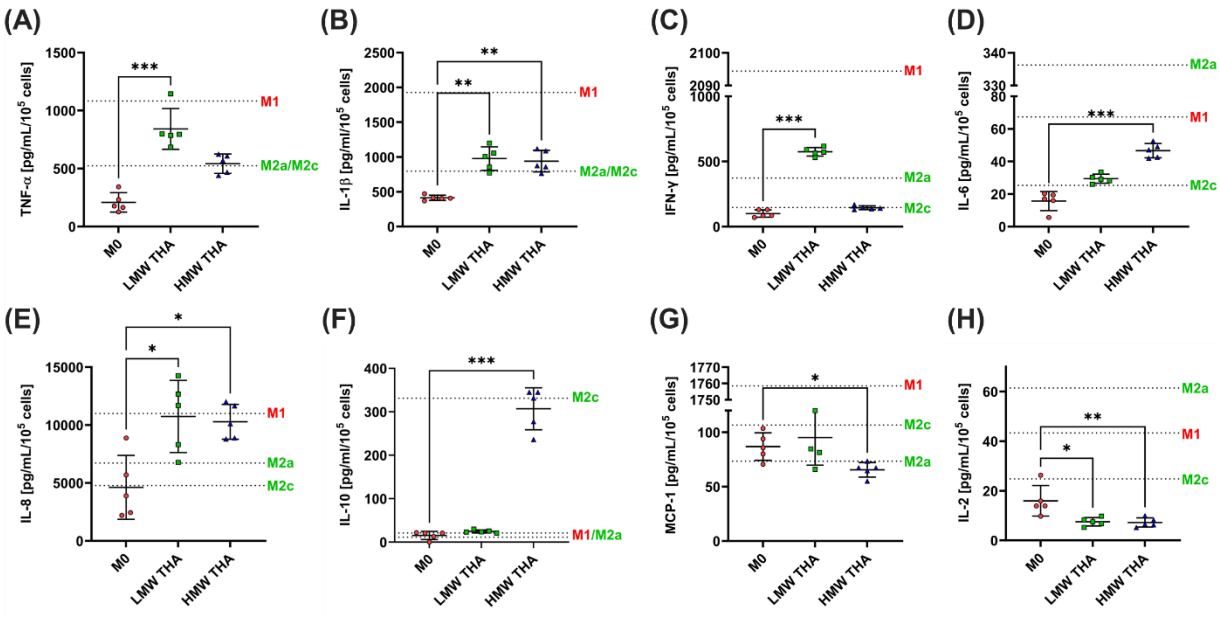

Figure 2. Cytokine secretion profile using multiplex bead-based ELISA on THP-1 derived MΦs. *Significant changes were found only in 8 cytokines, presented here:* ***(A)*** *TNF-α,* ***(B)*** *IL-1β,* ***(C)*** *IFN-γ,* ***(D)*** *IL-6,* ***(E)*** *IL-8,* ***(F)*** *IL-10,* ***(G)*** *MCP-1,* ***(H)*** *IL-2. In all cases* ***(A), (B)****, and* ***(E)****, horizontal dashed lines depict average values for the control polarized MΦs obtained as indicated in methods section. Statistical analysis was done by Kruskal-Wallis multiple comparisons test. A statistically significant results were considered for p<0.05 (* - <0.05, ** - <0.01, *** - <0.005 and **** - <0.001).*

In the next step, we evaluated the secretion profiles of 13 most common cytokines released by MΦs using multiplex bead-based ELISA: IL-2, IL-4, IP-10 (CXCL10), IL-1β, TNF-α, MCP-1 (CCL2), IL-17A, IL-6, IL-10, IFN-γ, IL-12p70, IL-8 (CXCL8), and TGF-β1. Significant changes were found in eight of the tested cytokines:

- pro-inflammatory - TNF-α (***Figure 2A***), IL-1β (***Figure 2B***), *IFN-γ* (***Figure 2C***), IL-6 (***Figure 2D***), IL-8 (***Figure 2E***),
- anti-inflammatory - IL-10 (***Figure 2F***),
- regulatory – MCP-1(***Figure 2G***) and IL-2 (***Figure 2H***).

Higher levels of TNF-α (***Figure 2A***), IL-1β (***Figure 2B***), IFN-γ (***Figure 2C***), IL-8 (***Figure 2E***), and MCP-1 (***Figure 2G***) suggest that LMW-THA supplementation generated MΦs with pro-inflammatory phenotype and M1-like characteristics. These cytokines are typically associated with pro-inflammatory responses and activation of M1 MΦs. On the other hand, lower levels of IL-2 (***Figure 2H***) suggest a deviation from the typical M1 phenotype, as IL-2 is generally associated with T-cell activation and is not typically produced by M1 MΦs. Nevertheless, overall, the obtained cytokine profile suggests an M1-like pro-inflammatory phenotype for the MΦs supplemented with LMW THA and aligns with flow cytometry data, pointing towards partly deviated M1-like phenotype.

On one hand, similarly to LMW THA supplementation, HMW THA showed higher levels of IL-1β (***Figure 2B***) and IL-8 (***Figure 2E***), suggesting polarization towards a pro-inflammatory phenotype with M1-like characteristics. On the other hand, higher levels of IL-6 (***Figure 2D***) and IL-10 (***Figure 2F***) both suggest a deviation towards an M2-like phenotype

with anti-inflammatory and immunoregulatory functions. IL-6 can be produced by both M1 and M2 MΦs, while IL-10 is typically produced by M2b, M2c or M2d subtypes and it is associated with anti-inflammatory responses key for the remodelling of external matrix [61, 64]. This goes in line with lower levels of MCP-1(***Figure 2G***), which suggest a potential decrease in chemotactic activity and recruitment of monocytes/MΦs, which indicates a shift away from the pro-inflammatory M1 phenotype. Lower levels of IL-2 (***Figure 2H***) also suggest similarly to the LMW THA supplementation a potential deviation from the typical M1 phenotype. Overall, the cytokine profile for HMW THA supplementation suggests a mixed phenotype with characteristics of both M1 and M2 MΦs, possibly indicating a transitional or heterogeneous population of MΦs.

Wang and Bratlie provided guidelines for MΦ polarization as a function of used polymer chemistry properties [65]. They argued that chemistry leading to more H-bonding capacity and higher hydrophilicity stimulates MΦs towards an M1 state, whereas overall charge plays a role in M2 modulation. Given our observations we currently cannot decouple the exact role of the tyrosine-chemical modification on the obtained profiling and point out that to some extent it may be influencing the outcome. Considering data from both flow cytometry and Multiplex ELISAs, the LMW THA supplementation induces a more pro-inflammatory M1-like phenotype in the THP-1-derived MΦs, while the HMW THA supplementation leads to a more intricate profile with some features of both M1 and M2 phenotypes, suggesting either a heterogeneous population or a transitional state. The observed profiles for LMW and HMW THA are however generally consistent with what might be expected for the treatment with non-modified low molecular weight hyaluronic acid (LMW-HA) and high molecular weight hyaluronic acid (HMW-HA), respectively [34, 66, 67], indicating that the tyramine modification with low degree of substitution does not significantly alter HA's biological response.

3.3. Immunological effects exerted on human donor-derived PMBCs-derived MΦs

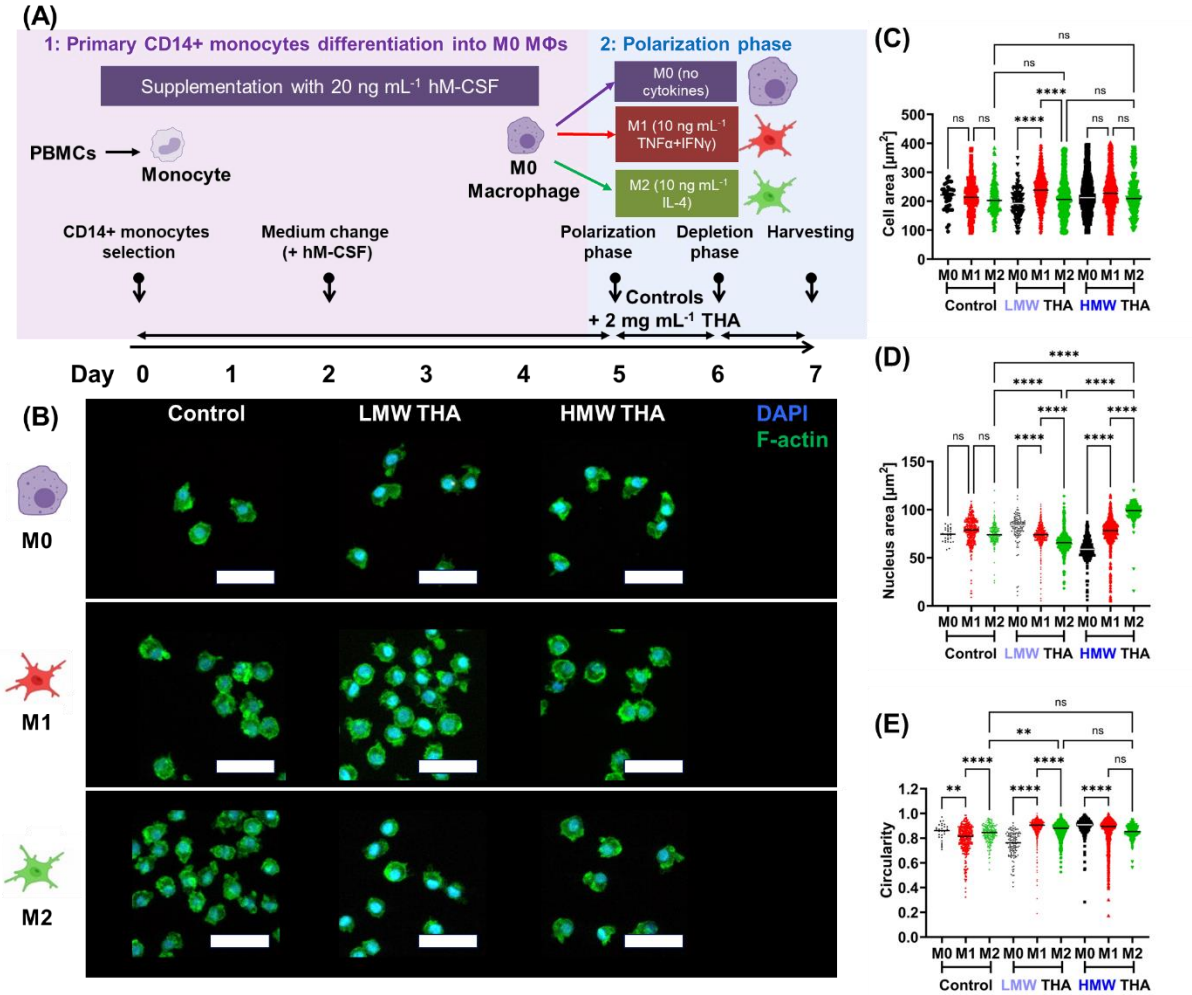

Figure 3. (A) Differentiation protocol and subsequent characterisation of peripheral blood mononuclear cells (PBMCs)-derived MΦs. *PBMCs were differentiated into M0 MΦs over 5 days period by supplementation with 20 ng mL^{-1} human macrophage colony-stimulating factor (hM-CSF). At day 5, differentiated M0 MΦs were polarized by medium supplemented with 10 ng mL^{-1} TNF-α and IFN-γ towards an M1 state and 10 ng mL^{-1} IL-4 towards an M2 state for 24 h, followed by a 24-hour rest in medium only, without supplementation. M0-like MΦs control samples were cultured in medium without any cytokines. The same three polarization states were maintained (M0, M1, M2), either without any addition (control), or in the presence of the 2 mg mL^{-1} LMW THA and HMW THA supplemented in the cell culture medium at day 5.* ***(B-E) Immunofluorescence characterisation of peripheral blood mononuclear cells (PBMCs)-derived MΦs. (B)*** *Immunofluorescence staining of nucleus by DAPI (**blue**) and F-actin by Phalloidin (**green**) for all tested groups. Images were digitally enlarged to higher magnification to enable visualization of individual cells. Original images with lower magnification are provided in supporting information **Figure S3**. Each raw represents different polarization state (M0, M1 and M2) and columns represent a control and samples supplemented with 2mg mL^{-1} LMW or HMW THA. Scale bar = 50 µm. ImageJ analysis of obtained for at least 100 cells for all groups of: **(C)** cell area, **(D)** nucleus area and **(E)** nucleus circularity. Analysis by one-way ANOVA with Šídák's multiple comparisons test. A statistically significant results were considered for p<0.05 (* - <0.05, ** - <0.01, *** - <0.005 and **** - <0.001).*

3.3.1. Cellular architecture parameters analysis

We then aimed to confirm the THP-1-derived MΦs polarisation obtained with supplementation of THA molecules on primary peripheral blood mononuclear cells (PBMCs)-derived MΦs (***Figure 3A***). Primary human-derived cells are generally recognized as more clinically relevant because they better preserve tissue characteristics [68]. This importance has also been noted for MΦs, albeit with their large heterogeneity [69, 70]. First, at day 6 of our protocol (***Figure 3A***) after the cytokine's depletion, we evaluated using bright field microscopy the preliminary changes in cellular shape as a function of all polarization states and supplemented THA (***Figure S3***). Indeed, qualitatively more elongated cells were obtained across biochemically induced M1 and M2 states, indicative of cellular changes. Moreover, more cellular protrusions (i.e. filopodia) were observed across all M1 groups, in line with previous observations for M1 type of MΦs [71, 72]. To confirm these findings, we firstly stained F-actin filaments and DAPI and performed immunofluorescence assay (on D1, from samples harvested from day 7 of polarization protocol) with semi-quantitative image analysis (***Figure 3B-E***). Fluorescent images confirmed similar findings that MΦs polarised biochemically *in vitro* to an M1 phenotype exhibited distinctly more lamellar processes, were of more elongated shape, whereas an M2 phenotype resulted in cells that were partly similar in shape to unpolarised M0 MΦs, with fewer lamellar processes. Furthermore, MΦs cultured in the presence of LMW THA appeared to have more filopodia and processes stemming from cellular bodies compared to control and HMW THA groups (***Figure 3B***). This trend has been confirmed with the significant differences in cellular areas between M0 and M1, and M1 and M2 groups ($p<0.001$, ***Figure 3C***), indicating a possible influence of LMW THA on the polarization state of obtained MΦs. A non-statistically significant trend for highest cellular area was observed for M1 phenotype, concurring with some previous observations [73]. For comparison, there were no significant differences noted for cells in either control or HMW

THA groups across all polarization states (***Figure 3C***). For control group, there were also no statistical differences in the area of nucleus between all polarization states (***Figure 3D***).

Currently there exists a small number of studies directly comparing nucleus size among M0, M1, and M2 macrophage subtypes [72]. This report [72] suggests a possible decrease of nuclear area for M1 phenotypes, although no statistical significance was provided. Overall, while nucleus size variations between M0, M1, and M2 MΦ subtypes have not been extensively studied, it is plausible that differences in activation state and functional phenotype may influence nuclear characteristics. Some recent studies [74] have utilised artificial intelligence (AI) and image processing capabilities on large datasets of microscopical images from different MΦ polarization states. The authors suggested several descriptors (area, length, width, circularity, aspect ratio, roundness and solidity) of MΦ cellular morphology and indeed found significant differences noted between states. In our model, supplementation of LMW and HMW had a measurable influence, with nuclei area decreasing from M0 to biochemically induced state M1 and to M2 ($p<0.001$) in LMW THA group, and the nuclei area increasing from M0 to biochemically induced state of M1 and to M2 in the presence of HMW THA (***Figure 3D***), showing opposing trends for LMW and HMW THA groups.

The AI-based study of multiple MΦ subtypes [74] has indicated that total cell circularity may be one of the key varied cellular factors for the M2a, but without significant differences noted between M1 and M0 groups; however, circularity of nucleus across different MΦ subtypes was not evaluated. In our case in the control group, the nucleus circularity of M1 MΦs was found lowest (***Figure 3E***, $p<0.01$), which concurred with previous observations of human primary MΦs on fibrous architectures [75]. On the other hand, this trend of nucleus circularity was modulated by the presence of LMW THA, with M0 group having lower nucleus circularity, similar to that of M1 in control group, indicating potential pro-inflammatory influence of LMW THA (***Figure 3E***). However, M1 group in LMW THA retained higher

nucleus circularity, similar to M0 in control group. This indicates that the effects stemming from simultaneous supplementation of LMW THA and 10 ng mL^{-1} TNF-α and IFN-γ of polarization cytokines might be mitigating each other. Although this analysis provides useful insights into modulatory potential of M_w of THA, we acknowledge its effects may be limited and, in this case, donor (D1) specific. In future, we see approaches similar to [74] undertaken on much larger sets of obtained images and across multiple donors in a machine-learning approach in anticipation of elucidation of donor-specific features. This work is however out of the scope of the current manuscript.

3.3.2. M1 and M2 surface receptors analysis

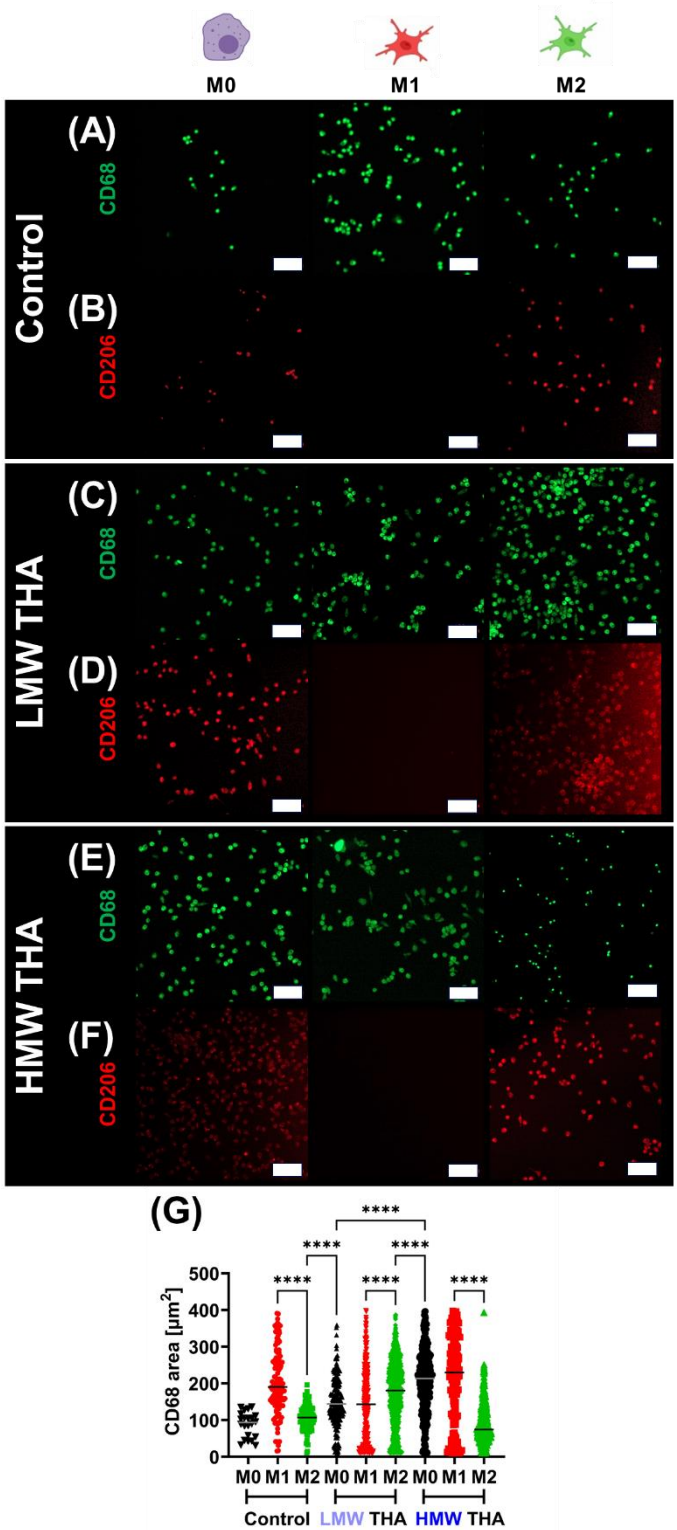

Figure 4. Surface marker characterisation of D3 peripheral blood mononuclear cells (PBMCs)-derived MΦs. Immunofluorescence *staining of CD68 (**green**) is shown in panels **(A)**, **(C)**, and **(E)**; whereas staining of CD206 (**red**) is shown in panels **(B)**, **(D)**, and **(F)**. Each column represents different polarization state (M0, M1 and M2) as indicated on the top. **(A)** and **(B)** represent panels for a control, **(C)** and **(D)** represent samples supplemented with 2mg mL^{-1} LMW THA, and **(E)** and **(F)** represent samples supplemented with 2mg mL^{-1} HMW THA. Scale bars for all images = 100 µm. All images containing full images including staining of nucleus by DAPI (**blue**) and F-actin by Phalloidin (**orange**) are presented in **Figure S5**. **(G)***

*ImageJ analysis of obtained images for all groups of CD68 area. Representative images are presented in **Figure 3A**, **C**, **E**, in main manuscript. Analysis by one-way ANOVA with Šídák's multiple comparisons test. A statistically significant results were considered for p<0.05 (* - <0.05, ** - <0.01, *** - <0.005 and **** - <0.001).*

To further investigate the propensity for M1 versus M2 polarisation in PMBCs-derived MΦs, we performed immunofluorescent staining using CD68, often associated as typical M1 marker [18, 76], and CD206 as M2 marker (***Figure 4***) [61, 77]. CD68 is typically located in the endosomal/lysosomal compartment however it has been shown to rapidly shuttle to the cell surface, particularly for M1 MΦ phenotype [18, 76]. In the control group, CD68 expression has been present in all polarization states mainly in endosomal compartment (M0, M1, M2, ***Figure 4A***), with its expression extending outside to the cell surface predominantely for M1-like phenotype, indicative of the pro-inflammatory polarization state. This is further supported by the largest CD68 staining area for M1 state across a control group (***Figure 4G***).

Our data on THP-1-derived MΦs suggests that CD206 is a downregulated receptor (***Figure 1E***) when supplemented with either LMW or HMW THA. However, differential regulation of CD206 expression between THP-1-derived MΦs and PBMCs-derived MΦs in response to a given supplementation could stem from a combination of differences in cellular origin, underwent mutations to achieve immortalization, differentiation status, MΦ subtype, genetic/epigenetic factors, as well as microenvironmental cues, hence we also evaluated expression of CD206 surface marker for PBMC-derived MΦs. Expression of CD206 was most evident in M2 polarization state in control group, with only some evidence of cells expressing it in M0 state (***Figure 4B***). M1 state did not show any expression of CD206, as expected for all the three tested groups (control, LMW and HMW THA). LMW THA was associated with stimulated expression of CD68 for M0 and M2 (non-significant, ***Figure 4C***, ***Figure 4G***). In all polarization groups, CD68 extended from endosomal compartment, with highest CD68 area in M2 state (***Figure 4G***). The area of CD68 and its overall expression appeared upregulated in

585 the presence of LMW THA (***Figure 4G***). On the other hand, LMW THA also induced
586 expression of CD206 in M0 group, potentially indicating a heterogenous population of MΦs in
587 this case (***Figure 4D***). As expected, no CD206 signal was observed in M1 state. In the M2
588 group, the CD206 signal appears, however partly diffused throughout sample, confirming that
589 LMW THA does not significantly suppress this expression in the presence of supplemented 10
590 ng mL^{-1} IL-4 (***Figure 4D***).

591 In M0 and M1 states, HMW THA we observed the CD68 expression extending from
592 endosomal compartments, whereas in M2 case, clearly more endosomal expression of CD68
593 was present (***Figure 4E*** and***4G***). On the other hand, M0 group supplemented with HMW THA
594 showed significantly higher area of CD68 staining than M2 group supplemented with LMW
595 THA ($p<0.001$), indicating predominance of HMW THA for expression of CD68 (***Figure 4G***).
596 However, this effect was significantly supressed by synergetic action with supplemented 10 ng
597 mL^{-1} IL-4, in which case clear retention of CD68 in endosomal compartment was evident, with
598 lowest area across all tested groups (***Figure 4G***), indicating a more synergetic pro-regenerative
599 action. This was further confirmed in CD206 staining, where there was relatively weak
600 expression for the M0 state, no expression in the M1 state and stronger expression in the M2
601 state (***Figure 4F***), in the presence of supplemented HMW THA.

602 Since our CD68 and CD206 staining is not co-localized (see Methods), we cannot
603 simultaneously quantify the same cells expressing both markers from our performed tests.
604 Hence, the immunocytochemistry results only point to the M2-like role of supplemented HMW
605 THA and somewhat more complex and heterogenous role of supplemented LMW THA
606 compared to the control groups. One limitation of our study is that the analysis was carried out
607 on one single donor (D3), with outlook towards envisaged AI/machine learning methods on a
608 much larger dataset of images in future. To unravel more complex dependence on multiple
609 donors, we next run RT-qPCR gene analysis of some of the common markers, including CD206

gene expression. Another limitation is that M-CSF, used in our study for macrophage maturation, has been reported to support a more M2-like phenotype [78-81]. Although controls without THA indicate that M1 polarization was successful in our model (***Figure 4A-B***), the results here reported might have been influenced using this growth factor instead of GM-CSF.

3.3.4. Gene expression analyses – intra versus inter-donor variability

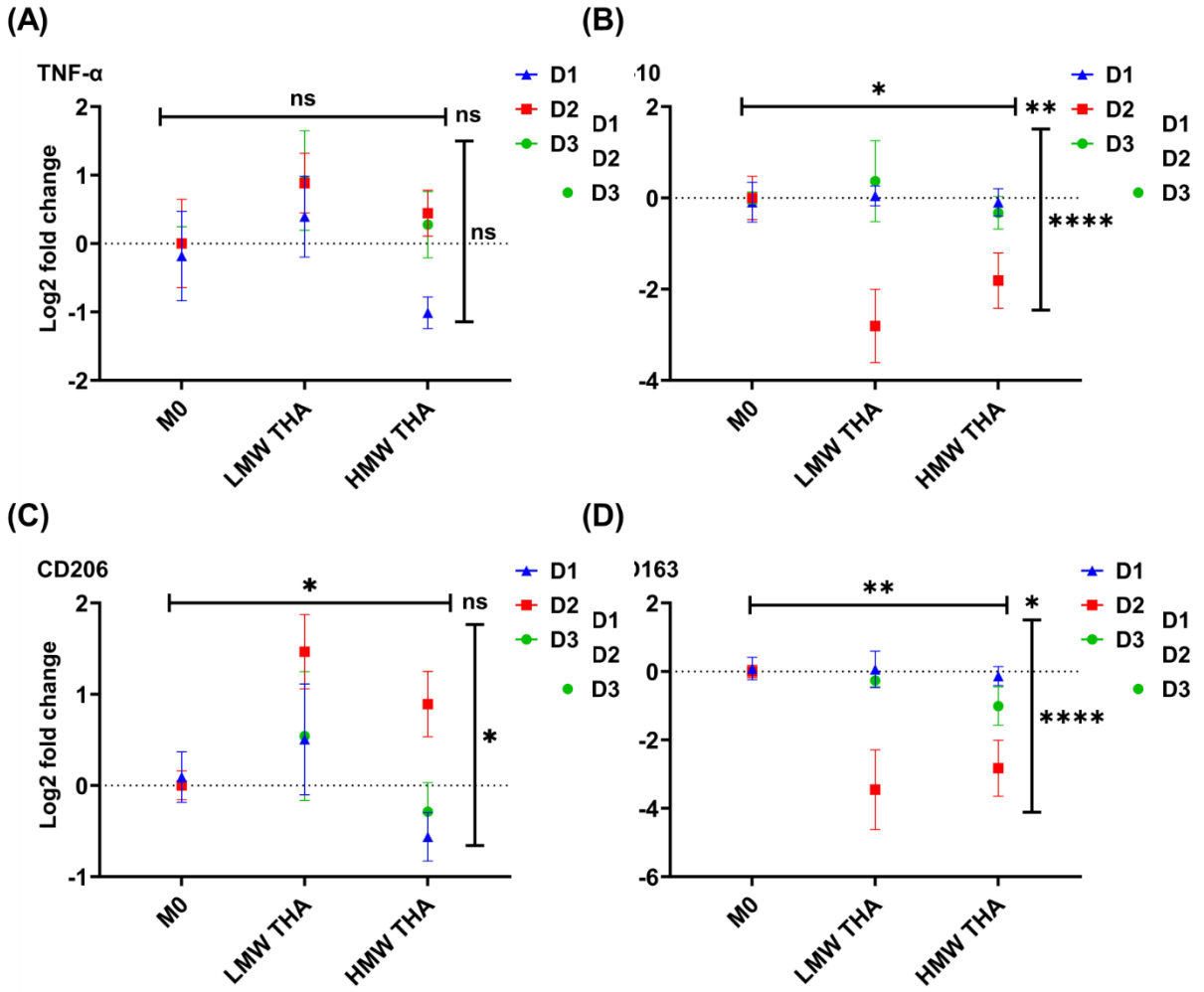

Figure 5. *Log2 fold change gene expression of* ***(A)*** *TNF-α,* ***(B)*** *IL-10,* ***(C)*** *MRC1 (CD206), and* ***(D)*** *CD163, measured by RT-qPCR for cells without any material conditioning (control) or encapsulated with 2 mg mL^{-1} LMW or HMW THA. Data represent average ± SD value from n=4 for D1 and n=3 for D2 and D3 from individual experiments. Gene expression is represented as fold change compared to RPLP0 (a housekeeping gene) of the M0 control group. Mixed effects model analysis with Geisser-Greenhouse correction was performed. A statistically significant results were considered for p<0.05 (* - <0.05, ** - <0.01, *** - <0.005 and **** - <0.001), with horizontal dash representing significance across supplementation/material, vertical across donors and corner value provides significance of their interaction.*

First, we evaluated a panel of markers (***Table 1***) consisting of pro-inflammatory markers (TNF-α, IL-6, IL-1β, iNOS), an anti-inflammatory marker (IL-10) and M2 surface markers (CD206 and CD163), on D1 samples (***Figure S6*** and ***Figure S7A, D, G***). Notably, although not significantly different, all M1 groups were characterized by the upregulation of TNF-α (***Figure S7A***). Out of all pro-inflammatory markers we only detected significant differences in TNF-α between all M1 groups (control, supplemented with both LMW and HMW THA) and M0 supplemented with HMW THA (***Figure S7A***), with no significant differences observed between any of the groups for the remaining pro-inflammatory markers (***Figure S6***). The M0 group supplemented with HMW THA had lowest values across all groups, suggesting the possible influence in its reduction of inflammation, as already showed by our investigations using THP-1 derived MΦs. We also did not detect any significant differences between any groups in anti-inflammatory IL-10 marker (***Figure S7D***), with only miniscule trends observed. We obtained slightly lower values for the M1 groups and slightly higher values for the M2 groups, in general in line with the expectations for the classical polarization. Finally, we saw clear trends in gene expression of CD206 surface markers, with downregulation of all M1 groups and upregulation of all M2 groups (***Figure S7G***). The only significantly detected differences were for M2 group supplemented with LMW THA, which appeared to have much higher expression compared to all M1 groups (***Figure S7G***). However, we do note the lack of statistical difference between any M2 groups.

Given the emerging picture of gene expression in D1 (which we run in first instance, ***Figure S6*** and ***Figure S7A, D, G***), to fully evaluate intra-donor variability, we then run full gene expression analysis on these four key markers: TNF-α, IL-10, CD206 and CD163, with the upregulated TNF-α predominantly representing M1 state, upregulated IL-10 and CD206 representing M2a and upregulated CD163 M2c state [82] on all three donors (***Figure 5*** and ***Figure S7***). The full individual panel of all markers is provided in ***Figure S7***, whereas here we

discuss general trends across all donors to confirm the overall effects of supplementation of THA molecules. Despite the fact that we observed upregulation in TNF-α, for LMW THA and downregulation for HMW THA, these were found not statistically significant across all donors (***Figure 5A***) as well as in mixed effects analysis. We could note slight tendencies of upregulation in M0 groups supplemented with LMW THA in all donors (not significant) (***Figure 5A***) concurring with the data obtained for THP-1-derived MΦs, but also possibly indicating weaker effects in PBMCs-derived MΦs. It appears that D1 seemed to differ from the other two donors. In D2 and D3 HMW THA supplementation had similar expression to M0 state (lack of significance, ***Figure 5A***). We also note that observed variations in regulation of TNF-α across donors may come from both environmental and genetic factors, including gender, white blood cells, tobacco consumption, and cholesterol levels **[83]**. These factors are not provided or controlled in the received blood donations, so drawing any decisive conclusions remains limited.

Unlike in the case of THP-1-derived MΦs where we measured high amount of released IL-10 from samples supplemented with HMW THA, for PBMCs-derived MΦs we did not observe any significant upregulation of IL-10 gene (***Figure 5B***). In fact, we observed lower expression of IL-10 for one donor (D2, ***Figure 5B***) when supplemented with both LMW and HMW THA. We also noticed some donor susceptibility to the typical biochemical induction of M1 and M2 states in the presence of LMW and HMW THA (***Figure S7E-F***). This, if anything, suggests a possible deviation from other M2 subtypes than M2a [61, 64]. One possibility is that THA of both M_w (***Figure 5E-F, Figure S7D-F***) influenced the typical JAK/STAT IL-10 production metabolic pathways in PBMCs-derived MΦs, and that certain donors may have propensity for this pathway's dysregulation [84] (***Figure 5B, Figure S7D-F***). The mixed effects statistics indicated significance across supplementation, donors and their interaction (***Figure 5B***). The interpretation of the overall IL-10 gene regulation data for PBMC-derived MΦs is complex as

human IL-10 regulation has been shown to be affected by interindividual variation in gene expression **[85, 86]**. We therefore believe that responses that we see in our data ($p<0.001$) stem directly from the variation introduced by host genetic factors, which are not pre-screened in received blood donations.

In the case of CD206 surface marker, we noted significance across supplementation and across donors, but not in their interaction (***Figure 5C***). For biochemically induced states, the CD206 upregulation was evident and coherent across all donors, with all M2 groups upregulated as compared to M1 groups (***Figure S7G-I***). By comparison of groups supplemented with LMW and HMW THA, in general LMW THA induced a slightly higher upregulation, whereas HMW THA variable regulation, with upregulation in D1 and downregulation in donors D2 and D3 (***Figure 5C***). In all cases differences are minimal. The data observed in the case of D2, for whom M0 group with supplemented LMW THA was upregulated, corroborated well with previously shown immunofluorescence staining (***Figure 4D***). Although CD206 is typically associated with M2a/M2c states of MΦ, it has been shown that its activation may also be associated with response to the overall inflammatory state [87], which may be the case of LMW THA for D1.

Finally, we also looked at the CD163 surface marker, where we noted, similarly to IL-10 case, significance in both supplementation, donor variation as well as their interaction (***Figure 5D***). Whilst D1 seemed not to respond to any supplementation, D2 showed downregulation of CD163 for both LMW and HMW THA, and D3 small downregulation for HMW THA (***Figure 5D***). These responses were even more pronounced in biochemically induced controls (***Figure S7J-L***) for donors 2 and 3.

The gene expression results corroborate to the observed fluorescence staining imaging obtained for the same donor D3 (***Figure 4*** and ***Figures 5*** **and** ***Figure S7***). In the overall picture, we observed that D2 had largest capacity to respond to the supplementation of both LMW and

HMW THA and that the generated MΦs appear to point towards a heterogenous state spanning some characteristics of M1 and some of M2a subtypes. We highlight that the gene expression experiments show difficulty of assessing the polarization states of PBMCs-derived MΦs supplemented with THA. Rather larger discrepancy is observed to the data obtained for the THP-1-derived MΦs, pointing out that differences in cellular origin, differentiation status as well as genetic/epigenetic factors being key in this case (with statistical significance noted across 3 tested genes for influence of donors). To further investigate the influence of THA supplementation, in the last step we evaluated cytokine expression by performing ELISAs on selected cytokines and donors.

3.3.5. Cytokine expression confirmation

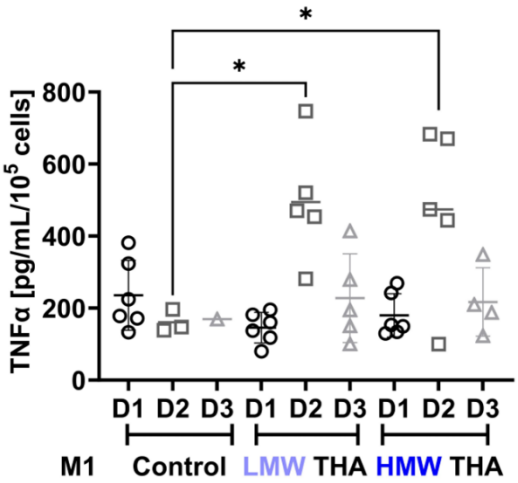

Figure 6. *TNF-α secretion measured by ELISA for cells without any material conditioning (control) or encapsulated with 2 mg mL^{-1} LMW or HMW THA, represented for each donor (D1, D2 and D3). Data is represented only for the M1 state, pre-stimulated by the addition of 10 ng mL^{-1} TNF-α and IFN-γ. The secretion for the other two cases (M0 and M2) in any other group was below the limit of detection, represented by the dotted line. Analysis by one-way ANOVA with Šídák's multiple comparisons test. A statistically significant results were considered for p<0.05 (* - <0.05, ** - <0.01, *** - <0.005 and **** - <0.001).*

Secretion of TNF-α was below the limit of detection (LoD) of 15.6 pg mL^{-1} for all M0 and M2 states across all groups (control, LMW and HMW THA), and was only evident in M1 groups of all donors (***Figure 6***), confirming expected most pro-inflammatory profile for the biochemically induced groups already discussed. For D1 and D3, there were no significant

differences between control, LMW or HMW conditions, whereas for D2, secretion of TNF-α was higher when supplemented with LMW and HMW THA, ($p<0.01$, ***Figure 6A***). This indicated a larger susceptibility of D2 to it and reaffirmed susceptibility observed in gene expression data for this donor (***Figure 5***).

We also evaluated secretion of IL-6, IL-10, IL-1β, and CD163 for D1, and IL-10 and CD163 for D2 and D3. For none of the donors we detected any IL-10 (with the LoD of 31.3 pg mL^{-1}), corroborating with the gene expression data showing no significant upregulation for any of the groups and polarization states. Combining above data for CD206 markers obtained for PBMC-derived MΦs, this indicates that speculatively these MΦs do not tend to polarize towards any other subtype than M2a. IL-1β for D1 also has not been detected for any of the groups (with LoD = 3.91 pg mL^{-1}). In D1, IL-6 was largely undetected (LoD=9.38 pg mL^{-1}) for control and HMW groups (***Figure S8A***), and only low amounts were detected in LMW THA group (in all states, M0, M1 and M2), perhaps pointing out to the slightly larger potential for pro-inflammatory induction of the supplemented LMW THA. For the CD163, we have detected none for D2 (LoD=156 pg mL^{-1}), and variable amounts for D1 (***Figure S8B***) and D3 (***Figure S8C***). The only statistically significant difference was observed between M1 control group and M0 supplemented with LMW THA in D1 (***Figure S8B***). On the other hand, no significant differences were observed between any polarisation states or groups in D3 (***Figure S8B***). This indicates that CD163, although often describing well the polarisation states, is strongly donor dependent for PBMCs-derived MΦs.

4. Conclusions

In summary here we unravel polarization tendencies of THP-1 and peripheral blood mononuclear cells (PBMCs)-derived MΦs upon supplementation with soluble chemically tyramine-modified hyaluronan (THA) at 2 mg mL^{-1} as biopolymer signals,

which constitute an important building block for many biomaterials or their released fragments. Flow cytometry and multiplex ELISA data on THP-1-derived MΦs indicate that supplementation with LMW THA induces a pro-inflammatory M1-like phenotype, whereas supplementation with HMW THA leads to a more intricate profile in THP-1 derived MΦs, with some features of both M1 and M2 phenotypes, suggesting either a heterogeneous population or a transitional state. On the other hand, in PBMCs-derived MΦs both LMW and HMW THA appear to induce this transitional M1 and M2 state, with high donor variability noted. This differential regulation of gene expression data between PBMCs-derived MΦs and expressed proteins and noted surface markers from THP-1-derived MΦs can stem from a combination of differences in cellular origin, genetic mutations to immortalize the cell line, differentiation status as well as genetic/epigenetic factors in received blood donor samples, which will require further analysis for better control. In principle, the effect of concentration of supplemented THA may also modulate the extent of already observed responses by us and remains a limitation of our study where single concentration was used.

In a general overview, LMW and HMW THA supplementation appears consistent with the possible expected profiles of non-modified hyaluronan, indicating that tyramine modification with low degree of substitution preserves HA immunomodulatory properties. This work contributes to bring biopolymer immunomodulation guidance to wider biomaterials and tissue engineering communities. We believe that these responses provide a useful representation and translational basis for the use of THA-based biomaterials in the future.

Author Contributions

J.K.W.: Conceptualization, data curation, formal analysis, funding acquisition, investigation, methodology, project administration, resources, supervision, validation, visualization, writing - original draft, writing – review & editing; **E.I.B.**: Data curation, investigation, methodology, writing – review & editing; **A.J.V.**: Data curation, investigation, methodology, writing – review & editing; **M.M.**: Data curation, investigation, methodology; **M.A.**: investigation, methodology; **P.S.T.**: Data curation, methodology; **J.S.** Data curation, investigation, methodology, formal analysis, writing – review & editing; **J.T.** Conceptualization, resources, funding acquisition, supervision, writing – review & editing; **D. E.**: Conceptualization, funding acquisition, supervision, writing – review & editing; **M.D.**: Conceptualization, funding acquisition, methodology, project administration, resources, supervision, writing – review & editing.

Funding sources

This work was supported by the European Union's Horizon 2020 (H2020-MSCA-IF-2019) research and innovation programme under the Marie Skłodowska-Curie grant agreement 893099 — ImmunoBioInks; by the Leading House for the Middle East and North Africa for Research Partnership Grant 2022 "Space ImmunoBioInks" (RPG-2022-38) and Consolidation 2023 "SI-WHIM" (COG-2023-35) grants. J.K.W. and M.D'E. also acknowledge the European Union's Horizon 2020 research and innovation programme under the grant agreement No 857287 (BBCE) as well as funding provided by AO Foundation.

Acknowledgements

The authors thank Nicolas Devantay for his technical support, particularly with the THA synthesis and Dr. Ursula Menzel for her assistance with PCR plating. The graphical abstract was created with BioRender.com.

Supplementary data

Supplementary data available: ^{1}H NMR spectra of synthesized THA; bright field microscopy images; NFκB-GFP fluorescence signals measured by flow cytometry; additional imageJ analysis and immunofluorescence images, detailed RT-qPCR gene analysis and ELISA results. Supplementary data to this article can be found online at XYZ.

Conflicts of interest

There are no conflicts to declare.

Notes

All research data supporting this publication are directly available within this publication and associated supporting information.

ORCID numbers of authors:

Jacek K. Wychowaniec: https://orcid.org/0000-0002-6597-5242

Ezgi Irem Bektas: https://orcid.org/0000-0002-3700-5708

Andrea J. Vernengo: https://orcid.org/0000-0002-5143-7435

Marcia Mürner: https://orcid.org/0009-0006-5305-2113

Paul Sean Tipay: https://orcid.org/0009-0002-9790-2598

Jiranuwat Sapudom: https://orcid.org/0000-0001-6627-7713

Jeremy Teo: https://orcid.org/0000-0001-6869-3833

David Eglin: https://orcid.org/0000-0002-8500-6887

Matteo D'Este: https://orcid.org/0000-0002-0424-8172

References

[1] K. Minton, Nature Reviews Immunology, 17 (2017) 277.

[2] C.H. Bucher, C. Schlundt, D. Wulsten, F.A. Sass, S. Wendler, A. Ellinghaus, T. Thiele, R. Seemann, B.M. Willie, H.-D. Volk, G.N. Duda, K. Schmidt-Bleek, Frontiers in Immunology, 10 (2019) 797.

[3] B. Zhang, Y. Su, J. Zhou, Y. Zheng, D. Zhu, Advanced Science, 8 (2021) 2100446.

[4] B. Shan, X. Wang, Y. Wu, C. Xu, Z. Xia, J. Dai, M. Shao, F. Zhao, S. He, L. Yang, M. Zhang, F. Nan, J. Li, J. Liu, J. Liu, W. Jia, Y. Qiu, B. Song, J.J. Han, L. Rui, S.Z. Duan, Y. Liu, Nat Immunol, 18 (2017) 519-529.

[5] S.R. Paludan, T. Pradeu, S.L. Masters, T.H. Mogensen, Nature Reviews Immunology, 21 (2021) 137-150.

[6] R. Rust, J. Kaiser, The Journal of neuroscience : the official journal of the Society for Neuroscience, 37 (2017) 4658-4660.

[7] J.C. Gensel, B. Zhang, Brain Research, 1619 (2015) 1-11.

[8] S. David, A. Kroner, Nat Rev Neurosci, 12 (2011) 388-399.

[9] K.A. Kigerl, J.C. Gensel, D.P. Ankeny, J.K. Alexander, D.J. Donnelly, P.G. Popovich, The Journal of Neuroscience, 29 (2009) 13435.

[10] P. Fang, X. Li, J. Dai, L. Cole, J.A. Camacho, Y. Zhang, Y. Ji, J. Wang, X.F. Yang, H. Wang, J Hematol Oncol, 11 (2018) 97.

[11] L. Chen, H. Deng, H. Cui, J. Fang, Z. Zuo, J. Deng, Y. Li, X. Wang, L. Zhao, Oncotarget, 9 (2017).

[12] G. Arango Duque, A. Descoteaux, Frontiers in Immunology, 5 (2014).

[13] T. Lawrence, G. Natoli, Nature Reviews Immunology, 11 (2011) 750-761.

[14] S. Gordon, 3 (2003) 23-35.

[15] S. Kobashi, T. Terashima, M. Katagi, Y. Nakae, J. Okano, Y. Suzuki, M. Urushitani, H. Kojima, Mol Ther, 28 (2020) 254-265.

[16] S.F. Ma, Y.J. Chen, J.X. Zhang, L. Shen, R. Wang, J.S. Zhou, J.G. Hu, H.Z. Lü, Brain Behav Immun, 45 (2015) 157-170.

[17] Peter J. Murray, Judith E. Allen, Subhra K. Biswas, Edward A. Fisher, Derek W. Gilroy, S. Goerdt, S. Gordon, John A. Hamilton, Lionel B. Ivashkiv, T. Lawrence, M. Locati, A. Mantovani, Fernando O. Martinez, J.-L. Mege, David M. Mosser, G. Natoli, Jeroen P. Saeij, Joachim L. Schultze, Kari A. Shirey, A. Sica, J. Suttles, I. Udalova, Jo A. van Ginderachter, Stefanie N. Vogel, Thomas A. Wynn, Immunity, 41 (2014) 14-20.

[18] M.H.M. Barros, F. Hauck, J.H. Dreyer, B. Kempkes, G. Niedobitek, PLOS ONE, 8 (2013) e80908.

[19] C.M. Walsh, J.K. Wychowaniec, L. Costello, D.F. Brougham, D. Dooley, Adv Healthc Mater, 12 (2023) e2300951.

[20] P. Wang, Y. Zhang, H. Lei, J. Yu, Q. Zhou, X. Shi, Y. Zhu, D. Zhang, P. Zhang, K. Wang, K. Dong, J. Xing, Y. Dong, Carbohydr Polym, 316 (2023) 121018.

[21] Q. Xiao, C.K. McAtee, X. Su, Nat Rev Immunol, 22 (2022) 188-199.

[22] J. Lu, J. Qian, Z. Xu, S. Yin, L. Zhou, S. Zheng, W. Zhang, Front Cell Dev Biol, 9 (2021) 631486.

[23] C.M. Walsh, J.K. Wychowaniec, D.F. Brougham, D. Dooley, Pharmacol Ther, 234 (2022) 108043.

[24] M.A. Wesdorp, A. Schwab, E.I. Bektas, R. Narcisi, D. Eglin, M.J. Stoddart, G. Van Osch, M. D'Este, Bioact Mater, 20 (2023) 627-637.

[25] A. Garcia-Garcia, S. Pigeot, I. Martin, Bioact Mater, 24 (2023) 174-184.

[26] J. Sapudom, M. Kongsema, A. Methachittipan, S. Damrongsakkul, S. Kanokpanont, J.C.M. Teo, M. Khongkow, K. Tonsomboon, P. Thongnuek, J Mater Chem B, 11 (2023) 3607-3616.

[27] B.P. Toole, Nature Reviews Cancer, 4 (2004) 528-539.

[28] K. Salma-Ancane, A. Sceglovs, E. Tracuma, J.K. Wychowaniec, K. Aunina, A. Ramata-Stunda, V. Nikolajeva, D. Loca, Int J Biol Macromol, 208 (2022) 995-1008.

[29] M. Halperin-Sternfeld, A. Pokhojaev, M. Ghosh, D. Rachmiel, R. Kannan, I. Grinberg, M. Asher, M. Aviv, P.X. Ma, I. Binderman, R. Sarig, L. Adler-Abramovich, J Clin Periodontol, 50 (2023) 200-219.

[30] W. Guo, L. Douma, M.H. Hu, D. Eglin, M. Alini, A. Secerovic, S. Grad, X. Peng, X. Zou, M. D'Este, M. Peroglio, Carbohydr Polym, 277 (2022) 118828.

[31] Q. Wei, Z. Jin, W. Zhang, Y. Zhao, Y. Wang, Y. Wei, X. He, G. Ma, Y. Guo, Y. Jiang, Z. Hu, Carbohydr Polym, 303 (2023) 120469.

[32] K.L. Aya, R. Stern, Wound Repair and Regeneration, 22 (2014) 579-593.

[33] D.-M. Kuang, Y. Wu, N. Chen, J. Cheng, S.-M. Zhuang, L. Zheng, Blood, 110 (2007) 587-595.

[34] B.C. Quartey, J. Sapudom, M. ElGindi, A. Alatoom, J. Teo, Adv Healthc Mater, n/a (2023) e2303125.

[35] T. Kobayashi, T. Chanmee, N. Itano, Biomolecules, 10 (2020) 1525.

[36] C. Yang, M. Cao, H. Liu, Y. He, J. Xu, Y. Du, Y. Liu, W. Wang, L. Cui, J. Hu, F. Gao, Journal of Biological Chemistry, 287 (2012) 43094-43107.

[37] J.E. Rayahin, J.S. Buhrman, Y. Zhang, T.J. Koh, R.A. Gemeinhart, ACS Biomaterials Science & Engineering, 1 (2015) 481-493.

[38] B.M. Lee, S.J. Park, I. Noh, C.H. Kim, Biomater Res, 25 (2021) 27.

[39] D.B. Lyle, J.C. Breger, L.F. Baeva, J.C. Shallcross, C.N. Durfor, N.S. Wang, J.J. Langone, Journal of Biomedical Materials Research Part A, 94A (2010) 893-904.

[40] L.F. Baeva, D.B. Lyle, M. Rios, J.J. Langone, M.M. Lightfoote, Journal of Biomedical Materials Research Part A, 102 (2014) 305-314.

[41] C.K. Hee, D.J. Messina, Journal of Immunology and Regenerative Medicine, 17 (2022) 100065.

[42] Y. Dong, A. Arif , M. Olsson, V. Cali, B. Hardman, M. Dosanjh, M. Lauer, R.J. Midura, V.C. Hascall, K.L. Brown, P. Johnson, Scientific Reports, 6 (2016) 36928.

[43] H. Kim, J. Cha, M. Jang, P. Kim, Biomater Sci, 7 (2019) 2264-2271.

[44] D. Petta, A.R. Armiento, D. Grijpma, M. Alini, D. Eglin, M. D'Este, Biofabrication, 10 (2018) 044104.

[45] K.S. Kim, S.J. Park, J.A. Yang, J.H. Jeon, S.H. Bhang, B.S. Kim, S.K. Hahn, Acta Biomaterialia, 7 (2011) 666-674.

[46] C. Loebel, S.E. Szczesny, B.D. Cosgrove, M. Alini, M. Zenobi-Wong, R.L. Mauck, D. Eglin, Biomacromolecules, 18 (2017) 855-864.

[47] R. Wang, X. Huang, B. Zoetebier, P.J. Dijkstra, M. Karperien, Bioact Mater, 20 (2023) 53-63.

[48] L.-S. Wang, F. Lee, J. Lim, C. Du, A.C.A. Wan, S.S. Lee, M. Kurisawa, Acta Biomaterialia, 10 (2014) 2539-2550.

[49] A. Schwab, C. Helary, R.G. Richards, M. Alini, D. Eglin, M. D'Este, Mater Today Bio, 7 (2020) 100058.

[50] M.M. Temple-Wong, S. Ren, P. Quach, B.C. Hansen, A.C. Chen, A. Hasegawa, D.D. D’Lima, J. Koziol, K. Masuda, M.K. Lotz, R.L. Sah, Arthritis Research & Therapy, 18 (2016) 18.

[51] D. Van der Heide, L.P. Hatt, E. Della Bella, A. Hangartner, W.A. Lackington, H. Yuan, F. De Groot-Barrère, M.J. Stoddart, M. D'Este, Carbohydrate Polymer Technologies and Applications, 7 (2024) 100518.

[52] C. Loebel, M. D'Este, M. Alini, M. Zenobi-Wong, D. Eglin, Carbohydrate Polymers, 115 (2015) 325-333.

[53] S.H. Rhee, Intest Res, 12 (2014) 90-95.

[54] J. Sapudom, W.K.E. Mohamed, A. Garcia-Sabate, A. Alatoom, S. Karaman, N. Mahtani, J.C. Teo, Bioengineering (Basel), 7 (2020) 33.

[55] J. Sapudom, S. Karaman, W.K.E. Mohamed, A. Garcia-Sabaté, B.C. Quartey, J.C.M. Teo, npj Regenerative Medicine, 6 (2021) 83.

[56] F. Razzi, L.E. Fratila-Apachitei, N. Fahy, Y.M. Bastiaansen-Jenniskens, I. Apachitei, E. Farrell, A.A. Zadpoor, Biomed Mater, 15 (2020) 035017.

[57] L. Utomo, G.S.A. Boersema, Y. Bayon, J.F. Lange, G. van Osch, Y.M. Bastiaansen-Jenniskens, Biomed Mater, 12 (2017) 025006.

[58] U.D.o.H.a.H. Services., F.a.D. Administration., C.f.D.E.a. Research., C.f.B.E.a. Research., C.f.V. Medicine., C.f.D.a.R. Health., O.o.R.A. (ORA). in: U.S.D.o.H.a.H. Services (Ed.), Food and Drug Administration, 2012.

[59] T. Liu, L. Zhang, D. Joo, S.-C. Sun, Signal Transduction and Targeted Therapy, 2 (2017) 17023.

[60] Y. Zhi, H. Lu, Y. Duan, W. Sun, G. Guan, Q. Dong, C. Yang, Int J Mol Med, 35 (2015) 349-357.

[61] J. Sapudom, S. Karaman, W.K.E. Mohamed, A. Garcia-Sabate, B.C. Quartey, J.C.M. Teo, NPJ Regen Med, 6 (2021) 83.

[62] A. Shapouri-Moghaddam, S. Mohammadian, H. Vazini, M. Taghadosi, S.A. Esmaeili, F. Mardani, B. Seifi, A. Mohammadi, J.T. Afshari, A. Sahebkar, J Cell Physiol, 233 (2018) 6425-6440.

[63] J. Lee, H. Tam, L. Adler, A. Ilstad-Minnihan, C. Macaubas, E.D. Mellins, PLOS ONE, 12 (2017) e0183594.

[64] J. Sapudom, X. Wu, M. Chkolnikov, M. Ansorge, U. Anderegg, T. Pompe, Biomaterials Science, 5 (2017) 1858-1867.

[65] D. Wang, K.M. Bratlie, ACS Biomaterials Science & Engineering, 1 (2015) 166-174.

[66] C.L.O. Tiah, B. Jasmin, D. Louise, C.d. Kergariou, T. Ash, W.P. Adam, B. Asme, bioRxiv, (2024) 2024.2004.2010.588451.

[67] S.M. Ruppert, T.R. Hawn, A. Arrigoni, T.N. Wight, P.L. Bollyky, Immunologic Research, 58 (2014) 186-192.

[68] M. Richter, O. Piwocka, M. Musielak, I. Piotrowski, W.M. Suchorska, T. Trzeciak, Frontiers in Cell and Developmental Biology, 9 (2021).

[69] F. Ginhoux, A. Mildner, E.L. Gautier, A. Schlitzer, C. Jakubzick, C. Varol, C. Bain, P. Guermonprez, Frontiers in Immunology, 11 (2021).

[70] B.K. Stansfield, D.A. Ingram, Clinical and Translational Medicine, 4 (2015) 5.

[71] P. Pelegrin, A. Surprenant, The EMBO Journal, 28 (2009) 2114-2127.

[72] H.M. Rostam, P.M. Reynolds, M.R. Alexander, N. Gadegaard, A.M. Ghaemmaghami, Sci Rep, 7 (2017) 3521.

[73] R. Sridharan, B. Cavanagh, A.R. Cameron, D.J. Kelly, F.J. O'Brien, Acta Biomater, 89 (2019) 47-59.

[74] M. Selig, L. Poehlman, N.C. Lang, M. Völker, B. Rolauffs, M.L. Hart, Frontiers in Immunology, 14 (2024).

[75] C. Mondadori, A. Chandrakar, S. Lopa, P. Wieringa, G. Talo, S. Perego, G. Lombardi, A. Colombini, M. Moretti, L. Moroni, Bioact Mater, 21 (2023) 209-222.

[76] D.A. Chistiakov, M.C. Killingsworth, V.A. Myasoedova, A.N. Orekhov, Y.V. Bobryshev, Laboratory Investigation, 97 (2017) 4-13.

[77] G.F. Vasse, P.T. Kühn, Q. Zhou, S.A. Bhusari, C. Reker-Smit, B.N. Melgert, P. van Rijn, Journal of Immunology and Regenerative Medicine, 1 (2018) 13-20.

[78] D.C. Lacey, A. Achuthan, A.J. Fleetwood, H. Dinh, J. Roiniotis, G.M. Scholz, M.W. Chang, S.K. Beckman, A.D. Cook, J.A. Hamilton, The Journal of Immunology, 188 (2012) 5752-5765.

[79] I. Ushach, A. Zlotnik, Journal of Leukocyte Biology, 100 (2016) 481-489.

[80] E. Van Overmeire, B. Stijlemans, F. Heymann, J. Keirsse, Y. Morias, Y. Elkrim, L. Brys, C. Abels, Q. Lahmar, C. Ergen, L. Vereecke, F. Tacke, P. De Baetselier, J.A. Van Ginderachter, D. Laoui, Cancer Research, 76 (2016) 35-42.

[81] A. Kelly, A.M. Grabiec, M.A. Travis, Culture of Human Monocyte-Derived Macrophages, in: G. Rousselet (Ed.) Macrophages: Methods and Protocols, Springer New York, New York, NY, 2018, pp. 1-11.

[82] P. Italiani, D. Boraschi, Frontiers in immunology, 5 (2014) 514.

[83] N. Haddy, C. Sass, S. Maumus, B. Marie, S. Droesch, G. Siest, D. Lambert, S. Visvikis, European Journal of Human Genetics, 13 (2005) 109-117.

[84] K.L. Singampalli, S. Balaji, X. Wang, U.M. Parikh, A. Kaul, J. Gilley, R.K. Birla, P.L. Bollyky, S.G. Keswani, Front Cell Dev Biol, 8 (2020) 636.

[85] C. Hedrich, J. Bream, Immunologic research, 47 (2010) 185-206.

[86] L.K. Kozicky, S.C. Menzies, Z.Y. Zhao, T. Vira, K. Harnden, K. Safari, K.L. Del Bel, S.E. Turvey, L.M. Sly, Front Immunol, 9 (2018) 2676.

[87] P.B. Wright, E. McDonald, A. Bravo-Blas, H.M. Baer, A. Heawood, C.C. Bain, A.M. Mowat, S.L. Clay, E.V. Robertson, F. Morton, J.S. Nijjar, U.Z. Ijaz, S.W.F. Milling, D.R. Gaya, Sci Rep, 11 (2021) 19616.